ADVANCED MATERIALS TECHNOLOGIES
www.advmattechnol.de

Enhancing the Performance of Soft Actuators with Magnetic Patterns

Svenja Hermann, Pauline Butaud,* Jean-François Manceau,* Gaël Chevallier,* and Christophe Espanet**

This study presents a concept for a straightforward method to enhance the actuation performances of magneto-active elastomer membranes. The concept is based on a characteristic magnetization pattern and offers a solution to two major difficulties in the actuation of thin and mechanically soft magnetic actuators: the localization of actuation forces and the self-demagnetization. After the magnetization process, the membrane presents two regions with an oppositely oriented out-of-plane magnetization. The magnetized regions are separated by a transition zone which is called magnetic pole transition. Experimental investigations reveal a high magnetic flux density near the pole transition—even in the center of bidirectionally magnetized membranes—whereas the magnetic flux density of a uniformly magnetized membrane decreases toward the center. In additional experiments, membranes with both magnetization patterns are actuated by stiff permanent magnets. The resulting out-of-plane displacement of the bidirectionally magnetized membrane exceeds the displacement of the unidirectionally magnetized membrane by far. The investigations demonstrate that this enhancement stems from the presence of the magnetic pole transition. All experiments are reproduced using magnetic and magneto-mechanical numerical models; a good accordance between the results is achieved.

1. Introduction

With the increasing use of embedded devices and wearable haptics in everyday life, soft actuators have received more and more attention from the engineering community during the last few years. The size of the devices decreases and, as a result, the actuators' size also decreases. Furthermore, actuators become multifunctional, i.e., capable of self-monitoring their status and giving feedback about it. In order to fulfill the new tasks, an increasing number of actuators contain so-called smart materials—actuated directly by physical stimuli—as basic building blocks. The use of magnetic stimuli stands out for the actuation speed and the possibility of untethered actuation. In the context of integrated magnetic actuators, an intensively studied type of smart material is the magneto-active elastomer (MAE). The high number of MAE-based concepts in the fields of soft robotics[1–3] and microfluidics,[4–6] for example, shows the interest of the community in this material.

MAEs are composite materials consisting of magnetic particles which are embedded in an elastomer matrix. The composite is particularly suitable for use in soft actuators as it combines unusual material properties: it reacts to magnetic stimuli and has a low mechanical stiffness. Due to the low stiffness, magnetically induced forces are of the same order of magnitude as the elastic forces in MAEs enabling a deformation of an MAE in magnetic fields. MAEs can be divided into two groups according to their magnetic behavior. Magnetically soft S-MAEs[7]

S. Hermann
Institute of Structural Mechanics, Statics and Dynamics
TU Dortmund University
44227 Dortmund, Germany
E-mail: svenja.hermann@tu-dortmund.de

P. Butaud, G. Chevallier
FEMTO-ST
Applied Mechanics Department
Besançon 25000, France
E-mail: pauline.butaud@univ-fcomte.fr; gael.chevallier@univ-fcomte.fr

J.-F. Manceau
FEMTO-ST
Micro Nano Sciences and Systems Department
Besançon 25000, France
E-mail: jfmanceau@femto-st.fr

C. Espanet
Moving Magnet Technologies SA
Besançon 25000, France
E-mail: christophe.espanet@movingmagnet.com

The ORCID identification number(s) for the author(s) of this article can be found under https://doi.org/10.1002/admt.202302142

DOI: 10.1002/admt.202302142

are magnetized only in the presence of an externally applied magnetic field. Magnetically hard H-MAEs[8] are permanently magnetized even in the absence of an external magnetic field. Interactions between an applied magnetic field and the particles generate mechanical loadings in the form of body forces and torques in the MAE. The forces pull the composite in the direction of the positive field gradient while the torques tend to align the magnetization with the direction of the external field.[9,10] In the absence of the magnetically induced loading, the elastic forces elastomer matrix restores the initial state of an MAE structure.

A magnetic actuation offers the possibility to obtain distributed loading with varying directions and intensities throughout the MAE. Several studies consider the control of the local magnetic loading as a key factor for the development of advanced actuation mechanisms and efficient miniature MAE actuators.[1,11] One strategy to achieve local loading is the use of the field gradient that naturally occurs with increasing distance from permanent magnets[12,13] or electromagnets,[14,15] for example. The local control of an applied magnetic field, however, can involve complex and space-consuming experimental setups.[16,17] This is why a large number of studies have recently focused on the design of MAE structures or on programming them[18] to achieve a distributed load.

Another strategy to achieve local loading is based on magnetic torques for the actuation. In S-MAEs, torques are generated when the distribution of the magnetic particles—and, thus, the magnetic properties—is anisotropic, as, for example, in a transversely isotropic microstructure. When the particles are aligned in chains[11,19] or filaments of magnetic composites with different orientations[20] are comprised in the S-MAE, the preferred direction of magnetization is along the chains of filaments. Magnetic torques occur when this direction is not aligned with the direction of the applied magnetic field. A deformation of corresponding S-MAEs can be achieved by uniform magnetic fields which is unfeasible for S-MAE with randomly dispersed particles.[21,22]

In H-MAE, a non-uniform magnetization (magnetization pattern) can be used to generate magnetic torques for the actuation. Magnetization patterns can be obtained, for example, by exposing an MAE to a unidirectional, strong magnetic field while it is maintained in a deformed shape.[23–25] After the magnetization, the specimen recovers its initial shape by elastic forces and shows multiple directions of magnetization. When immersed into a unidirectional magnetic field, the specimen deforms such that it resembles the deformed configuration due to the magnetic torques. It is also possible to align the direction of magnetization of pre-magnetized particles during 3D printing processes with external fields.[26,27] Printing the magnetization patterns, however, reduces the permanent magnetization by ≈35% compared to a magnetization after polymerization.[26] Magnetic patterns can also be generated by the external magnetic field during the magnetization.[28]

H-MAEs with magnetization patterns have been used to demonstrate shape memory effects in uniform external fields[23,26] and to achieve different types of movement of soft robots.[24,27] The actuation of the aforementioned structures, however, requires only weak actuation forces as the structures were able to move almost freely. Mechanically constrained actuators like membranes, are mainly actuated at the center while the outer contour is fastened, require higher actuation forces. In order to generate high actuation forces at the center of the membrane, rigid permanent magnets can be embedded in silicone matrices. Compared to this approach, H-MAEs can achieve higher displacements with less stress concentration.[29,30]

This study is a proof-of-concept study introducing a method to enhance the magnetic actuation capacity of H-MAE membranes. The concept relies on a magnetization pattern that reduces the self-demagnetization of the membrane and localizes the magneto-mechanical loading. To prove the concept, we compare an H-MAE membrane with the enhanced magnetization pattern to a membrane with a commonly used unidirectional magnetization. In the first step, the leakage flux density field of the two types of magnetized membranes is analyzed based on experimental measurements and numerical simulations. The results demonstrate the influence of the magnetic pattern on the self-demagnetization of the membrane in the air. To the best of our knowledge, this effect has not been considered in studies on thin H-MAE structures until now, even though it is an important factor for the actuation capacity. In the second step, the differently magnetized membranes are actuated with permanent magnets and the experiments are reproduced numerically. A comparison of the membranes' displacements highlights the advantage of a non-uniform magnetization for the actuation of H-MAE membranes.

2. Results and Discussion

2.1. Design of H-MAE Membranes with Magnetic Pattern

In order to demonstrate the force localization experimentally, two MAE membranes are prepared. NdFeB particles are mixed with a viscous silicone matrix such that a volume fraction of 36.2% is reached. A composite sheet of A4 size with a thickness of 1.5 mm is realized through molding and two membranes with a diameter of 24 mm are cut out using a circular die. SEM images show that the particles are randomly dispersed in the MAE and the quasi-static elastic modulus of the material is approximately 6 MPa. The magneto-active elastomer has a remanent flux density (B_r) of 300 mT. The coercive force H_c is comparatively high (940 kA m^{-1}) which means that the materials is difficult to demagnetize. More information about the raw materials and the synthesis of the MAE can be obtained in the Experimental Section of this study and Section S1 (Supporting Information).

The magnetic pattern presented in this study consists of two anti-parallel out-of-plane directions of magnetization as shown in **Figure 2a**. A transition zone with a width of 1 mm, called magnetic pole transition in the following, separates the two magnetized zones. In order to generate the magnetic pattern, a magnetization tool developed by the company Moving Magnet Technologies has been used. It generates a strong magnetic field which saturates the NdFeB particles in the membrane, and once the external field is switched off the particles remain magnetized due to their high coercive force. The magnetization device directs the magnetic field in two opposite directions in two neighboring regions (cf. Supporting Information) and thus generates the bidirectional pattern. A similar bidirectional magnetization can be achieved by placing a folded membrane in a unidirectional magnetic field (cf. ref. [31] for examples of folded MAE structures). The advantage of the magnetization tool is the constant width of

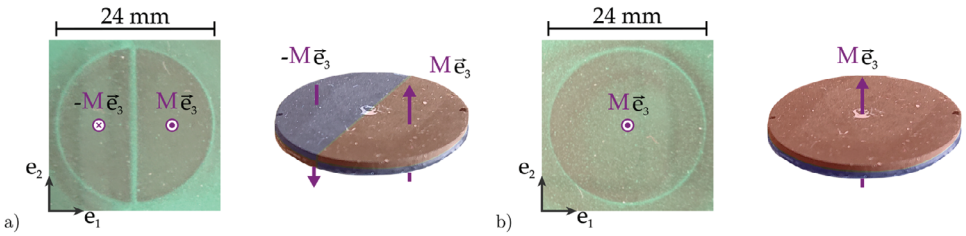

Figure 1. Illustration of the magnetization patterns. Top view on magnetic paper fixated onto the magnetized membrane (left) and perspective view of the membrane (right). The magnetization vector $\pm M\vec{e}_3$ is represented in purple and the conceptual magnetic poles are highlighted in red and blue respectively for the membranes with a) bidirectional and b) unidirectional magnetization.

the pole transition; the transition zone is slightly larger at the outside of the folded membrane than at the inside. We compare the membrane with bidirectional magnetization to a membrane with a commonly studied unidirectional magnetization (cf. Figure 2b). During the magnetization, this membrane is exposed to a strong unidirectional magnetic field in a coil.

The magnetization of the MAEs is verified prior to the experiments with the help of a magnetic paper that is placed on top of the membranes. The paper allows to visualize the intensity of the magnetic flux density (B) generated by the membrane: the lighter the color the higher the intensity. **Figure** 1a,b shows that the intensity of B is high near the outer edge of both, the unidirectionally and the bidirectionally magnetized membrane respectively. In addition, a high flux density is also observed in the region of the pole transition of the bidirectionally magnetized membrane Figure 1b. The reason for the uneven distribution is the demagnetization field inside the membrane that reduces its capacity to generate magnetic fields in regions where the magnetic flux cannot form closed loop easily (Supporting Information). The magnetic paper shows that the pole transition allows the membrane to concentrate the magnetic flux in regions of the membrane other than its outer edges.

2.2. Magnetic Flux Density Distribution

To analyze the magnetic flux density emitted by the differently magnetized membranes, the magnetic flux density is measured with a Hall sensor. The sensor is displaced at a distance of 1.4 mm above the membranes and in a measurement plane of 30 × 30 mm in steps of 1 mm (Figure 2a). A description of the experimental setup used for this purpose can be found in the Experimental Section of this study and Section S2 (Supporting Information).

The experimental results of the flux density component perpendicular to the membrane surface (B_3) in the measurement area are presented in Figure 2c. The measurement results confirm the results obtained with the magnetic paper. The flux density is highest near the edges of both membranes and around the pole transition of the bidirectionally magnetized membrane. The reason is the self-demagnetization (cf. ref. [32] for example) which is stronger in the centers of uniformly magnetized regions than near the outer edges. In addition, the use of the Hall sensor allows to quantify the intensity and determine the orientation of the magnetic flux density component B_3.

For the unidirectionally magnetized membrane, the magnetic flux density is distributed axisymmetrically due to the uniform magnetization and the geometry of the membrane: starting from the center of the membrane, B_3 increases with the radius toward the outer edge. On the contrary, the flux density in the center of the bidirectionally magnetized membrane is determined by the magnetic pole transition. The intensity of the flux density is lowest in the center of each of the two magnetized regions and increases the closer one gets toward the edges. The highest flux density is measured in the regions where the pole transition meets the edge of the membrane.

Concerning the orientation of B_3, the inversion of the latter near the outer bounds and the pole transition is clearly visible for both membranes. An illustration of the orientation is given by the dots in Figure 2d. They represent the values of B_3 obtained in the direction e_1 for a fixed x_2, indicated by the same dots in Figure 2c. Compared to the unidirectionally magnetized membrane, the pole transition allows to achieve a higher intensity of B_3. Furthermore, the flux density is slightly higher near the pole transition than near the outer edge of the bidirectionally magnetized membrane. Another characteristic is the high field gradient near the pole transition, where the direction of the magnetic flux is inverted over a short distance.

The experimental results are confirmed by a numerical boundary element (BE) model as shown in Figure 2d. The membrane has been modeled in the "Magnetic Fields No Currents" module of Comsol Multiphysics. A linear magnetic material model with the parameters described earlier in the article has been used. The bidirectionally magnetized membrane was separated into two inversely magnetized parts and a non-magnetized part for the pole transition. For the evaluation, the out-of-plane component of the magnetic flux density was calculated at the same distance and with the same discretization as in the experiment. The results show that the magnetic behavior of the membranes is well approximated with the chosen modeling assumptions. More information about the experimental setup can be found in the Experimental Section of the present study and in the Supporting Information.

In common membrane actuators, the membrane is fixed on the outer boundary and the central region is actuated. In this case, a bidirectional magnetization profile is advantageous for the actuation for several reasons. The central region shows a high intensity and a high gradient of the flux density which is favorable for a magnetic loading. Furthermore, the demagnetization field in the membrane center can be reduced by a magnetic pole transition as the magnetic flux can form closed loops easily around the transitions. The self-demagnetization gets stronger with the aspect ratio of the membrane, thin membranes, therefore, demagnetize easily in non-magnetic environments. Pole

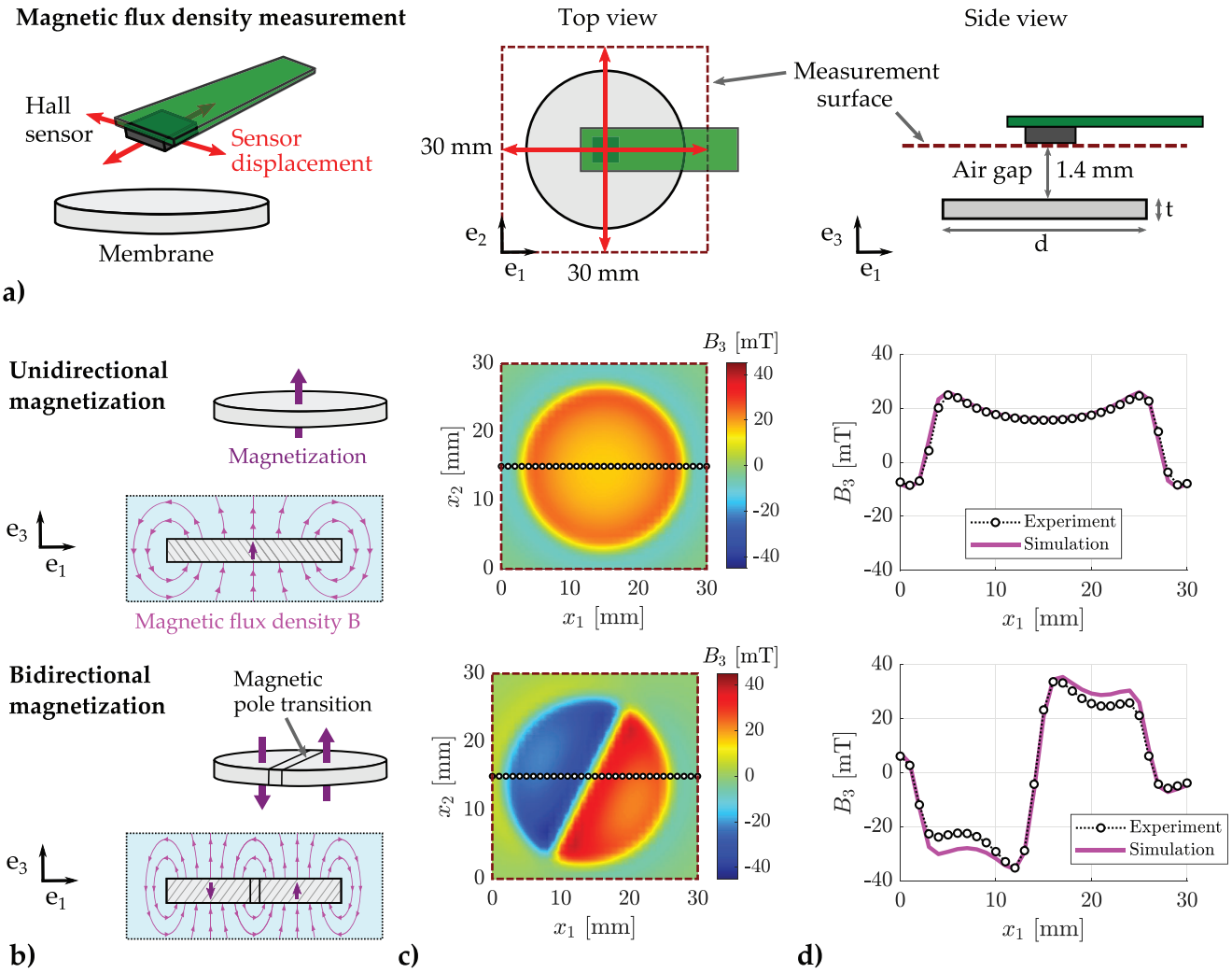

Figure 2. Evaluation of the magnetic flux density generated by the magnetized membranes. a) Schematic illustration of the experimental setup used to measure the out-of-plane component of the magnetic flux density $B_3 = \boldsymbol{B}\boldsymbol{e}_3$ (left) and scanning the area of the Hall sensor in the top view (center) and side view (right). b) Illustration of the magnetic flux density generated by the magnetized membranes with unidirectional (top) and bidirectional (bottom) magnetization. c) Measurement results of the magnetic flux density in the e_3 direction obtained in the $\boldsymbol{e}_1 - \boldsymbol{e}_2$ plane for the membranes with unidirectional (top) and bidirectional (bottom) magnetization. d) Comparison of the magnetic flux density in the $\boldsymbol{e}_3$ direction obtained from simulations and experimental tests at the locations marked with black dots in (c) for a unidirectional (top) and bidirectional (bottom) magnetization pattern.

transitions will allow to manufacture thin membranes with regions that stay magnetized in non-magnetic environments. The manufacturing of MAEs with multiple magnetic poles is, therefore, a relatively easy means to advance the miniaturization of magnetized MAE membranes.

2.3. Magneto-Mechanical Actuation

To compare their actuation capacities, both membranes are actuated with permanent magnets. During the experiments, the outer region of a membrane is fixed while a central region with a radius of 20 mm is left free to deform. This configuration represents common boundary conditions for a membrane actuator. Two mechanically stiff permanent magnets with a diameter of 25 mm and a thickness of 1 mm are used for the actuation. The permanent magnets have a residual flux density of 1.3 T; they were magnetized in a similar way to the membranes: unidirectionally and bidirectionally (cf. Section S3, Supporting Information).

Figure 3a depicts the actuation and the displacement measurement. In the setup, a magnet is positioned under the membrane so that the regions with opposing magnetization face each other to achieve repulsive interactions. It can be moved with respect to the membrane in two orthogonal in-plane directions and its distance toward the membrane can be varied in the third orthogonal direction. The setup allows a minimum air gap of 1.4 mm between magnets and membranes. At this distance, the magnet can generate a maximum flux density of 150 mT (out-of-plane direction) in the air. When the membrane is deformed by the interactions with the magnet, a surface scan with a numerical microscope allows to capture the deformed configuration from the top. The transverse displacement of

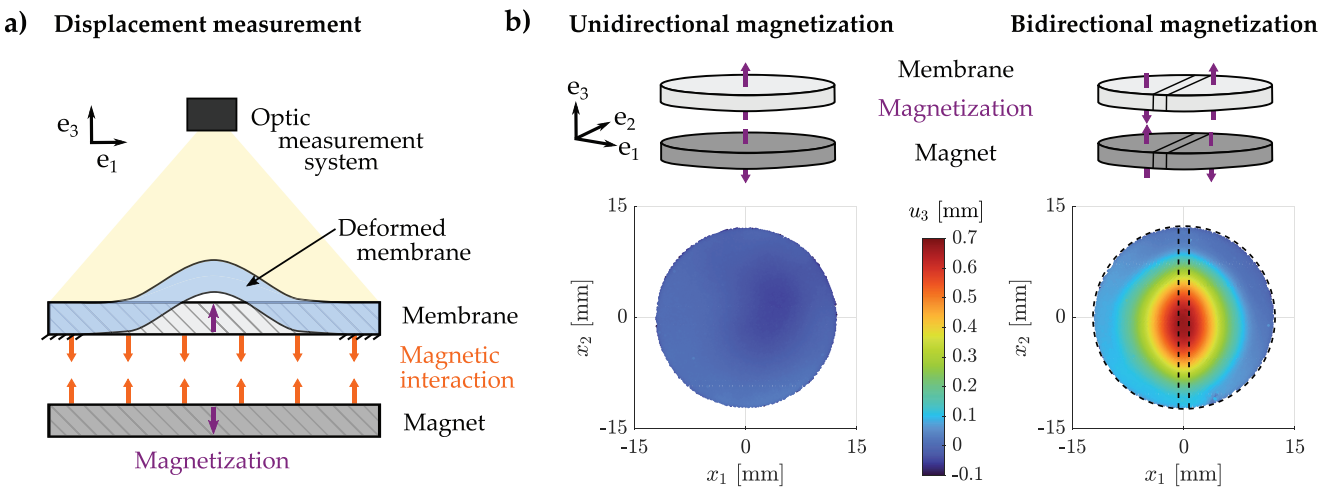

Figure 3. Evaluation of the membrane displacement generated by magnetic interactions between the magnetized membranes and stiff permanent magnets. a) Schematic representation of the measurement setup used to measure the out-of-plane component of the membrane displacement $u_3 = ue_3$. b) Measurement results for u_3 (bottom) obtained for the membrane with unidirectional (left) and bidirectional (right) magnetization patterns respectively. The corresponding magnetization patterns are illustrated above the measurement results.

the membrane (u_3) is calculated from the difference of the surface scans in the deformed and the initial states of the membrane. More information about the experimental setup and the post-processing of the data to obtain u_3 can be found in the Experimental Section of this study and Section S3 (Supporting Information).

In the first test, the axis of the magnet and the membrane were aligned and the air gap was set to the minimum. The membrane displacement was measured on the entire surface and the results are shown in Figure 3b. The displacements of the bidirectionally magnetized membrane exceed the displacement of the unidirectionally magnetized membrane by a large extend. The test results for the membrane with bidirectional magnetization indicate that the actuation takes place mainly around the magnetic pole transition. The displacement is symmetrically identical with respect to the transition zone (central dashed lines in Figure 3b), and also perpendicular to this direction.

The deformed shape of the membranes is confirmed with numerical finite element (FE) models implemented in Comsol Multiphysics. In the following, we refer to the model of the bidirectionally magnetized membrane. The magnet and the membrane are modeled with symmetry boundary conditions that allow to represent only half of the geometries. The additional boundary conditions correspond to the experimental configuration. The magnetic and the mechanical governing equations are assumed linear. The magneto-mechanical coupling is established on the surface of the membrane by the help of the Maxwell stress tensor (cf. Section S4, Supporting Information). **Figure 4** shows displacement field $\hat{u}_3$, normalized with respect to the maximum amplitude, which was obtained for the bidirectionally magnetized membrane. The localization of the displacement in proximity of the pole transition is clearly visible.

To confirm the role of the transition zone in the actuation capacities of the bidirectionally magnetized membrane, the

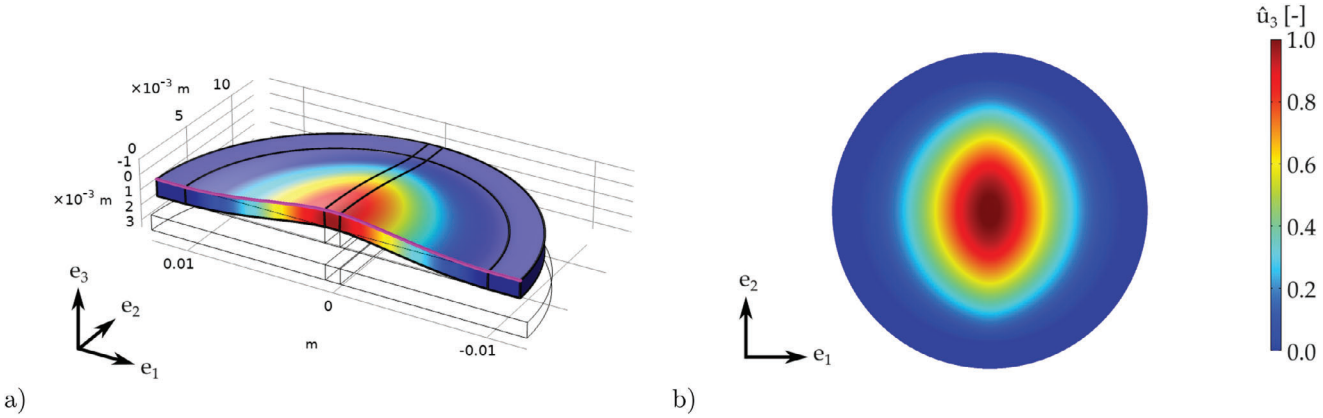

Figure 4. Normalized out–of–plane displacement field $\hat{u}_3 = u_3/\max(u_3)$ of the bidirectionally magnetized membrane obtained from a numerical simulation with a FE model. a) FE model of the membrane and the stiff permanent magnet (sectional view) where $\hat{u}_3$ is highlighted in color and the membrane is shown in the deformed state; the pink line illustrates the locations on which the out-of-plane displacement is qualitatively evaluated (cf. Figure 5). b) Top view on the normalized displacement field at the membrane top surface.

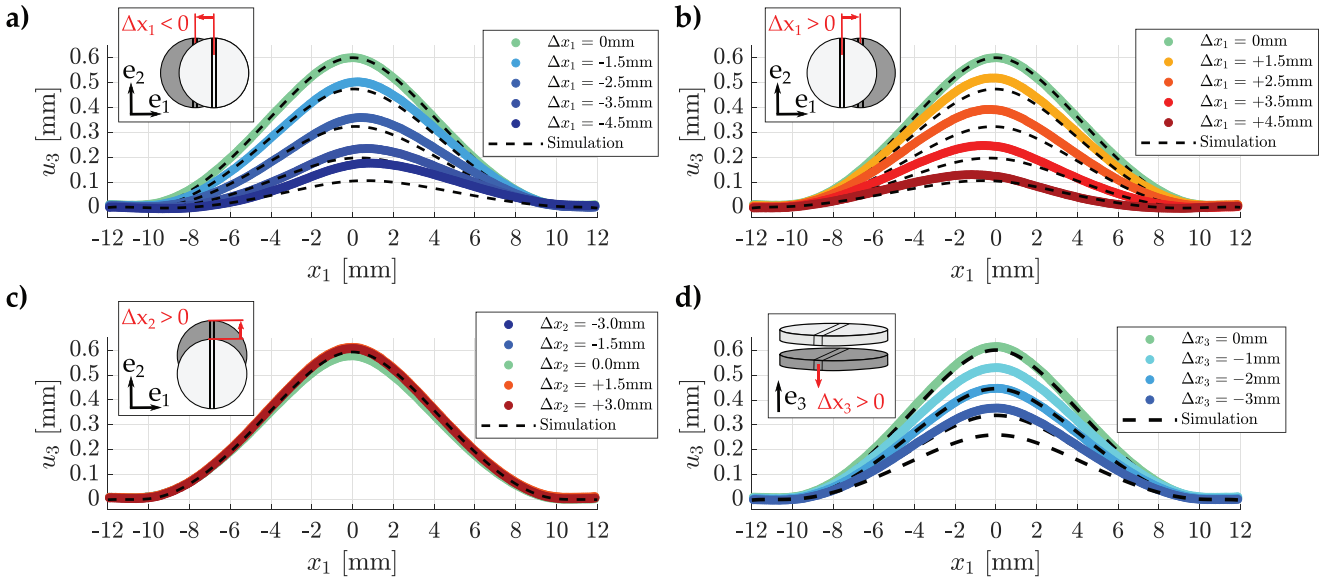

Figure 5. Comparison of the membrane's out-of-plane displacement u_3 obtained from experiments and numerical simulations for the bidirectional magnetization pattern. The actuation magnet was misaligned in different spatial directions with respect to the membrane for the tests: misalignment of the magnetic pole transitions in a) negative $\boldsymbol{e}_1$ direction and b) positive $\boldsymbol{e}_1$ direction, c) misalignment in positive $\boldsymbol{e}_2$ direction—the magnetic pole transitions of magnet and membrane keep facing each other—and d) misalignment in positive $\boldsymbol{e}_3$ direction corresponding to an increase in the air gap.

magnet was moved in two in-plane directions with respect to the membrane. For this test, the displacement measurement was performed in a reduced area of ± 0.5mm around $x_2 = 0$ in the direction e_1 (cf. Section S3, Supporting Information). The magnet was moved along the axis perpendicular to the pole transition in two directions at first. **Figure** 5a,b show that the membrane displacement decreases significantly with a misalignment of the pole transitions. Furthermore, the displacements become non-symmetric as the magnetic configuration is no longer symmetric due to the misalignment.

On the contrary, similar variations of the magnet position in the direction of the pole transition have no influence on the deformation of the membrane as shown in Figure 5c. This conclusion is limited to the position interval of the tests since a further displacement of the magnet would ultimately lead to configurations in which the magnet is no longer facing the membrane. When the distance between the magnet and the membrane increases, the magnetic actuation fields decrease and the deformation decreases as a consequence. This effect is shown in a test with an increasing air gap (Figure 5d).

The experimental tests show that the forces are concentrated around the region near the pole transition. The results are confirmed by numerical simulations of the experiment as shown in Figure 5a–d. Using the previously described numerical implementation, the magnet was positioned similarly to the experimental configuration and the results were obtained on the edge represented by the pink line in Figure 4a.

Using the elastic properties of the H-MAE allows a precise prediction of the displacements for small air gaps and symmetric arrangements of membrane and magnet. The simulations become less precise for configurations where the local magnetic quantities are more difficult to determine, i.e., a strong misalignment of the pole transitions and big air gaps. The role of the pole transition in the actuation mechanism of the membrane is hence confirmed experimentally and by numerical simulations.

Force localization offers two main advantages. From a magnetic point of view, the self-demagnetization of magnetized H-MAE is reduced near the pole transition, therefore even structures with a high aspect ratio remain magnetized. Additionally, the pole transition generates a strong local field gradient which offers the possibility to localize the magneto-mechanical loading, a characteristic which is increasingly sought in the field of soft magnetic actuators.

Results on MAE membrane actuation can be found in the literature, however, they are difficult to compare because important actuation parameters—listed in the following—are often very different among the various studies:

1. Raw material parameters: particle type (magnetically hard or soft) and elastomer stiffness
2. Structural parameters: particle content (trade-off between membrane stiffness and response to magnetic stimuli), particle distribution (isotropic or anisotropic), membrane geometry (i.e., bending stiffness), and mechanical boundary conditions
3. Magnetic parameters: actuation mean (magnet or coil), magnetic field intensity, magnetic field distribution (e.g., flux guidance by a magnetic circuit), and the size of the air gap

Table 1 shows a summary of different studies on MAE membrane actuators. The mere comparison of the out-of-plane displacement u_3 does not take into account the fact that the MAEs have different elastic moduli and geometries, i.e., different bending stiffnesses, different particle contents and different magnetic parameters. These examples illustrate the difficulties of a comparison of different study cases. In order to make a meaningful

Table 1. Comparison of membrane actuation results obtained in the present study and from the literature. u_3 – out-of-plane displacement, A – membrane surface, t – membrane thickness, E_{el} – elastic modulus of elastomer matrix, E_{MAE} – elastic modulus of MAE composite.

Reference	u_3 [mm]	At^{-1}[mm]	E_{el} [MPa]	E_{MAE} [MPa]	particles	vol[%]	mass[%]	air gap [mm]
Present study	0.6	301.9	1.4 [33]	6.84 [33]	NdFeB	36.2	80	1.4
[29]	0.009	215.6	0.75	–	NdFeB	6	–	3.0
[34]	1[a)]	143.6	–	0.55 – 0.85	NdFeB	–	75–85	1.0
[35]	0.253	8.0	1.0	–	Fe_3O_4	12.5	–	N/A
[36]	3	1413.7	0.0013 – 0.035 [5]	–	"Iron"	–	20	7.0

[a)] no indication about particle content for this result.

comparison between different cases, it is necessary to compare them under the same conditions. Regarding the present study, we can state that a bidirectional magnetization will greatly improve the actuation capacity of an H-MAE membrane.

3. Conclusion

In the present study, we introduce and prove a concept that enhances the magnetic properties and improves the actuation capacity of thin H-MAE membranes. The basis of the enhanced membrane's properties is the magnetization pattern consisting of three regions: two large regions which are inversely magnetized in the out-of-plane direction and a narrow region—the magnetic pole transition–separating the magnetized regions. Experimental investigations show that the magnitude of the magnetic flux density is almost doubled in the central region of the membrane compared to a commonly used unidirectional magnetization. The pattern reduces the self-demagnetization of the MAE membrane and, thus, enhances the capability of the membrane to respond to magnetic stimuli. Furthermore, the actuation capacity in the central region of the membrane is strongly increased, as experimental tests and numerical simulations show. The deformation of a membrane with a bidirectional magnetization pattern exceeds the displacement of a unidirectionally magnetized membrane to a large extent. We show that the improved actuation performance is due to the localization of the actuation forces around the magnetic pole transition.

In conclusion, this study demonstrates the potential magnetic patterns to localize the magnetic forces where they are needed for the actuation of a MAE membrane. Being able to place the pole transitions at locations where the actuation forces are required makes the membrane actuator more efficient and offers more freedom in the actuator design. Furthermore, the same base MAE material can be used for different actuator designs by simply changing the magnetization pattern to adapt the actuation conditions. In addition, the pattern enables H-MAEs with a high aspect ratio to stay magnetized which is an important aspect for the miniaturization of membrane actuators. The presented magnetization patterns can be reproduced without difficulty since the flexibility of the membrane allows the magnetization in a deformed configuration. We also show that the magnetic and magneto-mechanical the behavior of the MAE membrane can be reproduced with numerical models. Using the models will accelerate a further optimization of the actuation since different raw materials and geometries as well as specific actuation scenarios can be assessed in parametric studies with little effort. The development of patterns are similar to the ones presented in this study and, therefore, likely to advance the development of H-MAE actuators in the fields of microfluidics or soft robotics, for example.

4. Experimental Section

Raw Materials and Magnets: The H-MAE of this study was composed of a magnetically hard powder and a silicone matrix. The matrix consists of the elastomer MED-4014 was provided by NuSil. It was a two-part silicone that cured with heat via platin-catalyzed addition-cure chemistry. The ratio of the mixture of the two parts, A and B, was 1:1. In the uncured state, the consistency of the two parts could be compared to modeling clay. The cured silicone had a specific gravity of 1.08 (ASTM D792), a shore hardness of 15 (Durometer type A, ASTM D2240) and was transparent. The magnetic powder MQFP-14-12 consisted of NdFeB particles and was provided by Magnequench in a non-magnetized state. The average PSD50 value of the powder lies was 5.5 µm which means that the diameter of 50% of the particles was inferior or equal to this value. The powder was obtained by jet milling and the shape of the particles was irregular. The particles were magnetically isotropic, the residual flux density of the material measured 805 ± 20 mT and the internal coercive field strength H_c measured 965 ± 55 kA m^{-1}. The mass density of the material was 7620 kg m^{-1}. Details about the elaboration process of the H-MAE can be found in ref. [33]. The magnets, used in this study, were made from the magnetically hard material BMN-42SH. Specimens with a diameter of 25 mm were cut out from sheets with a thickness of 1 mm by electroerosion. The magnets were magnetically anisotropic and their residual flux density in the out-of-plane direction measured 1.3 T.

Magnetic Measurements: The test bench that was used for the measurement of the magnetic flux density was developed by the company MMT (cf. Section S3, Supporting Information). It consisted of a support part for the placement of the specimens and a triaxial magnetic Hall probe provided by the company Senis AG. The relative position of the probe and a specimen could be varied in three orthogonal directions. The probe was positioned by two-step motors, arranged in orthogonal directions, and the specimen was positioned by a third-step motor in the remaining spatial direction. In the present study, the sensing element had a distance of 1.2 mm toward the specimen surface during the measurements. The air gap was composed of the distance of the sensing element toward the surface of the sensor housing (1.0 mm, Z-axis of the probe) and the air gap between the housing and specimen surface (0.2 mm).

Magneto-Mechanical Measurements: The test bench used for the analysis of the membrane displacement consisted of two parts: the first part allows to vary the relative position of the rigid magnet with respect to the membrane in a magnetically neutral environment. The second part consisted of an optical measurement system, that recorded the out–of–plane displacement of the membrane, caused by magneto-mechanical interactions with the magnet. The membrane was fixed on an aluminum plate, which was supported by two pillars, made of acrylic glass. The aluminum plate had a circular opening with a diameter of 20 mm in the middle. This was the region, where the membrane was left free to deform. It was fixed

in the outer region (for $d > 20$ mm) to the aluminum plate with the adhesive Super Glue-3 from Loctite. The pole transition of specimens with bidirectional magnetization was aligned with the e_2 – direction of the experimental setup. All specimens were positioned on separate aluminum plates with a thickness of 1.2 mm.

The magnet was fixed on a supporting positioning part by the adhesive Super Glue-3. The position of the magnet was adjusted by the three connected micro-translation stages, type M-105 from Physik Instrumente (PI), each having a linear travel range of 18 mm and a minimum graduation step of 0.01 mm.

For the observation of the membrane displacement in the out-of-plane direction, a numerical microscope from Bruker alicona was used. The microscope was able to determine the absolute 3D coordinates of points on a surface that itself was displaced in the working area. To scan the surface of an object, the latter was moved in the orthogonal directions e_1 and e_2 by two linear stages while the microscope lens was displaced in the perpendicular e_3 – direction. To prevent a movement of the membrane with respect to the linear tables, the base plate of the mechanical part of the experimental setup was fixed to the upper linear tables with the help of screws. The enlarger lens with a magnification of 5x of the numerical microscope was used, a measurement resolution of 15 µm was chosen for the directions e_1 and e_2 and a resolution of 10 µm in the direction e_3. The lighting properties specified for the optical measurement were the brightness and the contrast which were set to 127µs and 0.51 in the software, respectively. Furthermore, a polarization filter has been used to improve the lighting of the relative mat MAE surface.

During this experiment, two types of measurements were performed. For a first time, a scan of the entire surface was carried out, but only once for each specimen due to the acquisition time (2 h) and the size of the output files. In subsequent analysis, only a part of the surface was scanned. A reduced scan was conducted in a volume including the full diameter of the membrane in direction e_1 and a range of ± 2 mm in the direction e_2. More details about the experimental setup and the data processing can be found in Section S3 (Supporting Information).

Supporting Information

Supporting Information is available from the Wiley Online Library or from the author.

Acknowledgements

This work was funded by the French company Moving Magnet Technologies SA and EIPHI Graduate School, ANR-17-EURE-0002. The authors would like to thank B. Guichardaz from the FEMTO-ST Institute for her support in creating the Table of Contents graphic.

Open access funding enabled and organized by Projekt DEAL.

Conflict of Interest

The authors declare no conflict of interest.

Data Availability Statement

The data that support the findings of this study are available from the corresponding author upon reasonable request.

Keywords

force localization, magneto-active elastomer, pole transition, soft membrane actuator

Received: December 12, 2023
Revised: April 12, 2024
Published online:

[1] N. Bira, P. Dhagat, J. Davidson, *Front. Robot. AI* **2020**, *7*, 146.
[2] Y. Chi, Y. Li, Y. Zhao, Y. Hong, Y. Tang, J. Yin, *Adv. Mater.* **2022**, *34*, 2110384.
[3] S. Leanza, S. Wu, X. Sun, H. Qi, R. Zhao, *Adv. Mater.* **2023**, *36*, 2302066.
[4] K. Oh, C. Ahn, *J. Micromech. Microeng.* **2006**, *16*, R13.
[5] J.-Y. Qian, C.-W. Hou, X.-J. Li, Z.-J. Jin, *Micromachines* **2020**, *11*, 172.
[6] W. Hilber, *Appl. Phys. A* **2016**, *122*, 1.
[7] M. Lokander, B. Stenberg, *Polym. Test.* **2003**, *22*, 245.
[8] G. Stepanov, A. Chertovich, E. Kramarenko, *J. Magn. Magn. Mater.* **2012**, *324*, 3448.
[9] A. Kovetz, *Electromagnetic theory*, Oxford University Press Oxford, **2000**.
[10] R. Zhao, Y. Kim, S. A. Chester, P. Sharma, X. Zhao, *J. Mech. Phys. Solids* **2019**, *124*, 244.
[11] J. Kim, S. E. Chung, S. E. Choi, H. Lee, J. Kim, S. Kwon, *Nat. Mater.* **2011**, *10*, 747.
[12] A. Diermeier, D. Sindersberger, G. Monkman, in *Conference ACTUATOR, Bremen (Germany), 2016*, **2016**, pp. 1–4.
[13] L. Miao, Y. Song, Z. Ren, C. Xu, J. Wan, H. Wang, H. Guo, Z. Xiang, M. Han, H. Zhang, *Adv. Mater.* **2021**, *33*, 2102691.
[14] K. Tao, J. Wu, A. Kottapalli, D. Chen, Z. Yang, G. Ding, S. Lye, J. Miao, *Solid-State Electron.* **2017**, *138*, 66.
[15] A. Paknahad, M. Tahmasebipour, *Microelectron. Eng.* **2019**, *216*, 111031.
[16] E. Diller, J. Zhuang, G. Zhan Lum, M. R. Edwards, M. Sitti, *Appl. Phys. Lett.* **2014**, *104*, 174101.
[17] L. Manamanchaiyaporn, T. Xu, X. Wu, *IEEE/ASME Trans. Mechatron.* **2020**, *25*, 2688.
[18] P. Sinha, T. Mukhopadhyay, *Mater. Sci. Eng. R: Rep.* **2023**, *155*, 100745.
[19] J. Voropaieff, Ph.D. thesis, Université Paris-Saclay, France, **2019**.
[20] S. Qi, H. Guo, J. Fu, Y. Xie, M. Zhu, M. Yu, *Compos. Sci. Technol.* **2020**, *188*, 107973.
[21] A. Singh, L. Hirsinger, P. Delobelle, C. Khan-Malek, *Microsyst. Technol.* **2014**, *20*, 427.
[22] G. Nanni, S. Petroni, D. Fragouli, M. Amato, M. De Vittorio, A. Athanassiou, *Microelectron. Eng.* **2012**, *98*, 607.
[23] G. Z. Lum, Z. Ye, X. Dong, H. Marvi, O. Erin, W. Hu, M. Sitti, *Proc. Natl. Acad. Sci.* **2016**, *113*, 6007.
[24] W. Hu, G. Z. Lum, M. Mastrangeli, M. Sitti, *Nature* **2018**, *554*, 81.
[25] X. Kuang, S. Wu, Q. Ze, L. Yue, Y. Jin, S. Montgomery, F. Yang, H. Qi, R. Zhao, *Adv. Mater.* **2021**, *33*, 2102113.
[26] Y. Kim, H. Yuk, R. Zhao, S. Chester, X. Zhao, *Nature* **2018**, *558*, 274.
[27] T. Xu, J. Zhang, M. Salehizadeh, O. Onaizah, E. Diller, *Sci. Rob.* **2019**, *4*, 29.
[28] Q. Ze, X. Kuang, S. Wu, J. Wong, S. Montgomery, R. Zhang, J. Kovitz, F. Yang, H. Qi, R. Zhao, *Adv. Mater.* **2020**, *32*, 1906657.
[29] M. Said, J. Yunas, R. Pawinanto, B. Majlis, B. Bais, *Sens. Actuators, A* **2016**, *245*, 85.
[30] Y. Zhou, F. Amirouche, *Micromachines* **2011**, *2*, 345.
[31] Z. Qi, M. Zhou, Y. Li, Z. Xia, W. Huo, X. Huang, *Adv. Mater. Technol.* **2021**, *6*, 2001124.
[32] B. D. Cullity, C. D. Graham, *Introduction to Magnetic Materials*, John Wiley & Sons, Hoboken, NJ **2011**.
[33] S. Hermann, P. Butaud, G. Chevallier, J.-F. Manceau, C. Espanet, *Smart Mater. Struct.* **2020**, *29*, 105009.
[34] Y. Kim, J. Lee, S.-M. Park, *Mater. Today Commun.* **2024**, *39*, 108705.
[35] M. Manzo, M. Bakaraju, *AIP Adv.* **2022**, *12*, 11.
[36] V. Jayaneththi, K. Aw, A. McDaid, *Smart Mater. Struct.* **2020**, *29*, 035010.